JCTC Journal of Chemical Theory and Computation

Ligand Field Effects on the Aqueous Ru(III)/Ru(II) Redox Couple from an All-Atom Density Functional Theory Perspective

Regla Ayala and Michiel Sprik*

Department of Chemistry, University of Cambridge, Lensfield Road, Cambridge CB2 1EW, United Kingdom

Received May 12, 2006

Abstract: The $[RuCl_6]^{4-}(aq) \rightarrow [RuCl_6]^{3-}(aq) + e^-$ and $[Ru(CN)_6]^{4-}(aq) \rightarrow [Ru(CN)_6]^{3-}(aq) + e^-$ half redox reactions are investigated using density functional based ab initio molecular dynamics methods. The aim is to understand at a microscopic level how the difference in π-bonding of these ligands is reflected in the redox chemistry. To this end, we have computed the redox and reorganization free energies using a method derived from the Marcus theory of electron transfer. The resulting estimate of the free energy change of the full redox reaction between the two coordination complexes is compared to experiment. Our findings indicate that ligand character has an important effect on the vertical ionization chemistry but less on the relaxation of the system after removal or addition of electrons. This enables us to correlate the redox free energies with the HOMO energy levels of the combined solute + solvent system and analyze the redox chemistry in terms of the corresponding energy level diagram.

1. Introduction

The response to removal or excitation of electrons of molecules in solution is determined ultimately by changes in total energy. However the microscopic understanding of such a process has been largely based on models of effective one-electron states of the solute species. The ligand field theory for transition-metal coordination complexes is a good illustration of the power of the orbital picture. Many of the chemical and physical properties of these systems can be rationalized in terms of energy levels and symmetries of the one-electron orbitals. The particular question that will concern us here is the effect of a change in the chemical nature of the ligands. Among various model systems used to study this question, ruthenium(II) and ruthenium(III) coordination complexes occupy a special place. The reason for this popularity is the huge variety of stable low spin complexes formed by these transition-metal ions and the corresponding wide range of accessible optical and electrochemical properties.[1−4]

The search for correlations between molecular orbitals (MOs) and electrochemical and optical characteristics of transition metal complexes was initially based on semiempirical electronic structure methods (see for example ref 4 and references therein). The smaller coordination complexes can now also be treated using self-consistent field methods. In particular density functional theory (DFT) has proven to be an efficient and (comparatively) reliable tool for electronic structure computation of transition metal complexes.[5,6] The effect of the solvent is usually modeled by a dielectric continuum[6−8] or cancels when special properties of similar complexes are compared (for example pK_a's of aqueous cations).[9] DFT based ab initio molecular dynamics (MD) methods[10] should "in principle" allow us to take a more fundamental approach and treat the redox active solute and solvent at the same level of electronic structure theory. Recent studies of aqueous trivalent aqua cations (Al^{3+}[11], Y^{3+}[12], Fe^{3+}[13],) indicate that this integral "ab initio" MD approach is capable of giving a realistic description of the hydration structure and dynamics of these species. Also the reactivity of the Fe^{3+} aqua-ion toward hydrogen peroxide has already been investigated.[14] However, in the present context such a scheme is only meaningful provided we are also able to compute redox potentials for these model systems. We have recently shown that for a subset of redox

* Corresponding author e-mail: ms284@cam.ac.uk.

10.1021/ct600169e CCC: $33.50
Published on Web 08/23/2006

reactions it is in fact possible to obtain reasonably accurate estimates of the reaction free energy change.[15−18] Our method is an ab initio MD implementation of the method originally developed by Warshel and co-workers[19−21] for molecular dynamics simulation of electron transfer in solution. The aqueous ruthenium cation, being a textbook example of a redox system in the linear response regime where Marcus theory applies, has played a crucial role in the development and validation of our method[15,17] (for a related study of the electronic absorption of this system see ref 22).

In the present work we apply the same ab initio MD approach to two aqueous ruthenium coordination complexes, $[Ru(CN)_6]^{4-}$ and $[RuCl_6]^{4-}$. These complexes can be regarded as a minimal model for the study of the effect of exchange of a ligand with π-acceptor (CN^-) for a ligand with π-donor character (Cl^-) (see for example refs 23 and 24). More specifically, the objective is to investigate the nature of the, in principle, extended DFT one-electron (Kohn−Sham) states produced by the ab initio MD calculation and interpret or, to use a spectroscopic analogy, assign these states in terms of ligand field theory. The first question is how the traditional picture of π-bonding is reflected in the actual Kohn−Sham orbitals of the extended solute + solvent system obtained from the ab initio MD trajectory. The next step is to correlate the orbital structure with the redox and reorganization free energies as computed for the $[RuCl_6]^{4-}(aq) \rightarrow [RuCl_6]^{3-}(aq) + e^-$ and $[Ru(CN)_6]^{4-}(aq) \rightarrow [Ru(CN)_6]^{3-} + e^-$ half reactions. As could be expected in view of the success of ligand field theory, our calculations verify that the occupied orbitals of the combined solute + solvent system conform to the ligand field theory picture. More surprising is that, for this particular system, the agreement extends even to a semiquantitative level, in that the difference in energy between the highest occupied molecular orbital (HOMO) of $[Ru(CN)_6]^{4-}$ and $[RuCl_6]^{4-}$ is found to be consistent with the computed reaction free energy change of the full $[RuCl_6]^{4-} + [Ru(CN)_6]^{3-} \rightarrow [RuCl_6]^{3-} + [Ru(CN)_6]^{4-}$ redox reaction. The final test will be to compare this value to experimental estimates.

The organization of the paper is as follows. Section 2 briefly summarizes the relevant ligand field theory and the Marcus theory based method for the computation of free energies. Technical details and parameters defining the density functional MD technique are also given in this section. Results are presented and discussed in section 3. Section 4 contains some concluding remarks putting this work in the more wider context of the computational study of the redox reactions.

2. Theory and Method

2.1. Ligand Field Theory. Coordination complexes of ruthenium in oxidation states II and III are very popular with both experimentalists and theorists. One reason is the preference of ruthenium for low spin octahedral structures, such as the $[RuCl_6]^{3/4\ -}$ and $[Ru(CN)_6]^{3/4\ -}$ anions studied here. The central metal ion in $Ru(II)L_6$ has formally a $4d^6$ configuration, which under low spin conditions, leads to full occupation of the t_{2g} levels of the complex (t_{2g}^6) and therefore to singlet spin multiplicity. Similarly, $Ru(III)L_6$ compounds

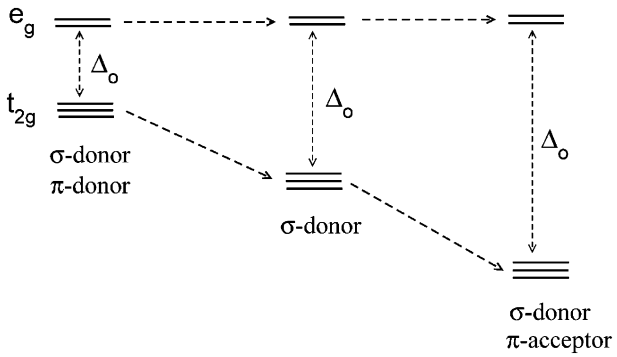

Figure 1. Schematic MO diagram of the response of the ligand field splitting Δ_o of an octahedral coordination complex ML_6 to change the π-bonding character of ligands L.

with one electron less (t_{2g}^5) are doublets. Another attractive feature is that most of these complexes are textbook examples of redox active species following outer-sphere redox kinetics as described by Marcus theory.[25−30] Perhaps the most well-known are Ru hexa-amines, $[Ru(NH_3)_6]^{2/3+}$, with one or more ammonia ligands replaced by aromatic molecules with nitrogen heteroatoms (pyridine, pyrazine, etc).[2] The well-behaved Marcus character of these complexes was also the reason we chose aqueous Ru hexahydrate ($[(Ru(H_2O)_6]^{2/3+}$) as the model system for the development and validation of the Marcus theory based ab initio MD methodology for the computation of redox potentials.[15,17]

The focus of the present application is less on the central metal atom, which is chosen for convenience, but on the Cl^- and CN^- ligands. Cl^- and CN^- are at opposite ends of the spectrochemical series giving rise to a different splitting of the manifold of *d*-orbitals. The ligand splitting due to 6-fold CN^- coordination can easily be in the 3 eV range or more, while the splitting for Cl^- is usually about half this value.[23] The standard explanation is that Cl^- is a π-donor ligand, while CN^- acts as a π-acceptor. The difference is in the mixing with the filled t_{2g} manifold (see Figure 1). These orbitals are not participating in the σ-bonding and retain predominantly metallic *d* orbital character. In the case of π donation from a lower lying ligand π orbital (a 3*p* lone pair for Cl^-) the t_{2g} orbitals acquire some antibonding character and are pushed up. This closes the gap with the (unoccupied) σ-antibonding e_{2g} levels which are not affected by π-bonding. Conversely, in the case of π-acceptor ligands, the t_{2g} states mix with a higher lying empty π^* orbital, become (weakly) bonding, and are as a result pushed down opening the gap with the e_{2g} manifold.

The orbital picture sketched above makes no mention of the environment of the complex. When the complex is embedded in a dielectric continuum or is part of a static ordered crystal, this is presumably not necessary, at least at the qualitative or semiempirical level. However, what will be the effect of the multitude of electronic levels and the thermal fluctuations in solution? The very fact that ligand field theory is also used in solution chemistry suggests that the orbital picture still applies. We will see that this expectation is justified, although the thermal fluctuations do add an extra dimension to the problem which can even be exploited in calculations (see section 2.2). Moreover, the

solvent effect, in a quantitative sense, can be substantial. This holds in particular for multiply charged anions such as $[Ru(CN)_6]^{3/4-}$ and $[RuCl_6]^{3/4-}$ which are unstable in the gas phase. At this point it should be mentioned that, while the Ru(II/III) hexacyanides are stable aqueous species, the Ru(II)/(III) chlorides are extremely labile as a result of rapid ligand−water exchange. In fact the hexachloride is not known in aqueous solution. However, on the ab initio MD time scale (≈10 ps) $[RuCl_6]^{3/4-}$ complexes can easily survive, and the use of this complex rather than a stable existing π-donor is a compromise imposed by the limitations in model system size (see also section 2.3). Fortunately for ruthenium complexes a comprehensive set of ligand additivity rules is available,[3,4] enabling us to make a reasonably accurate estimation of the hypothetical experimental reduction potential for the aqueous $[RuCl_6]^{3/4-}$ couple. This is what we will rely on in this computational study.

2.2. Free Energy Calculations. Marcus theory provides an ideal framework for the application of MD simulation to electron transfer (ET). Marcus theory[25−30] connects the ET driving force (reaction free energy change) and the free energy of activation with the diabatic total energy of the reacting species coupled to a solvent bath. The solvent is assumed to respond linearly to a change of charge of the solute. These assumptions lead to two overlapping quadratic free energy surfaces with equal curvature with respect to the reaction coordinate. The ET process occurs at the crossing point of the free energy surfaces. Warshel has converted this formulation in an efficient and elegant MD method for the study of ET reactions.[19,21] The key feature of the method is that it employs two potential energy surfaces: one potential energy surface (PES) for the reactant and one for the product system. The method has been applied in numerous model potential studies, either purely classical, with the potential energy surfaces derived from a force field model, or quantum with a Hamiltonian based on a empirical valence bond scheme.

The extension of the two surface approach to DFT should be in principle straightforward but is, in practice, seriously hampered by the well-known shortcomings in the DFT treatment of charge transfer. The implementation for half reactions $R \rightarrow O + e^-$, however, is less precarious from the DFT perspective, as we have shown in a series of recent papers.[15−18,31−34] The central quantity in this approach is the vertical ionization energy ΔE defined as the difference between the total energies $E_M(\mathbf{R}^N)$ of the oxidized (M = O) and reduced (M = R) system at fixed atomic configuration $\mathbf{R}^N$.

$$\Delta E(\mathbf{R}^N) = E_O(\mathbf{R}^N) - E_R(\mathbf{R}^N) \tag{1}$$

The key assumption of Marcus theory, in its microscopic formulation, is that the distribution of equilibrium fluctuations of ΔE in the reduced and oxidized states is Gaussian.[19] If this condition is satisfied, then the free energy change of oxidation

$$\Delta A = A_O - A_R \tag{2}$$

can be directly computed from the mean and variance of the vertical energy gap ΔE in oxidized and reduced states according to

$$\Delta A = \Delta E_O + \lambda \tag{3}$$

$$= \Delta E_R - \lambda \tag{4}$$

The MD estimates of ΔE_O and ΔE_R are computed by averaging the vertical energy gap of eq 1 over an equilibrium trajectory in the O respectively R state. λ in eqs 3 and 4 is obtained from the corresponding variance (second moment) σ_M^2, M = O, R of the gap fluctuations

$$\lambda = \frac{\sigma_O^{\,2}}{2k_BT} = \frac{\sigma_R^{\,2}}{2k_BT} \tag{5}$$

where k_B is the Boltzmann constant, and T is the temperature at which the MD simulations are carried out. The quantity λ can be equated (in the linear regime) with the free energy of reorganization (for more details of the development followed to obtain the above expressions see ref 16 and references therein). Linking the Marcus reorganization free energy to the variance of the gap fluctuations, eq 5 implies that this width is independent of the oxidation state. This equality is not an additional assumption but is a special property of Gaussian energy gap fluctuation.[16,19,35] In practice this symmetry is used as a criterion for the validity of the Marcus theory for a given system. It also allows us to eliminate the width in the expression for the oxidation free energy. Adding and subtracting eqs 3 and 4 gives

$$\Delta A = \frac{1}{2}(\Delta E_R + \Delta E_O) \tag{6}$$

$$\lambda = \frac{1}{2}(\Delta E_R - \Delta E_O) \tag{7}$$

It will be clear that the pairs of eqs 3, 4 and 6, 7, while mathematically equivalent, have a very different status from a MD point of view. A MD approach based on eqs 6, 7 requires two equilibrium trajectories, one on the oxidized PES ($E_O(\mathbf{R}^N)$ in eq 1) and one on the reduced PES ($E_R(\mathbf{R}^N)$). Equations 3 and 4 claim that the same information can be obtained from a simulation on just a single PES (either O or R), at the expense, however, of having to converge the second moment of the fluctuations of the energy gap (eq 5), which usually takes a significantly longer run than needed for an estimate of the expectation values ΔE_M. This is why the two-state scheme is preferred in practice. However, for reasons explained below, the free energy computations of the present study are based on the one-state scheme.

2.3. Model System Composition and Size. Model systems in the half reaction scheme as implemented in previous studies[15−18,31−34] consist of a periodically replicated cubic box containing 30−50 solvent molecules and a single redox active solute. No explicit counterions are included. Neutrality is restored by the background of a uniform charge distribution implicit in the Ewald treatment of long-range interactions in periodic systems. The same approach is also used in the present study. The length of the cubic cell is $L = 11.44$ Å. The cell contained one $[RuCl_6]^{4-}$ ($[Ru(CN)_6]^{4-}$) metal

Table 1: Reaction Free Energies in Units of eV of Four Model Redox Reactions Compared to Experiment[a]

redox reaction	solvent	ΔA(calc)	ΔG(exp)	ref
$Cu^{1+} + Ag^{2+} \rightarrow Cu^{2+} + Ag^{1+}$	water	−1.7	−1.82	31
$RuO_4^{2-} + MnO_4^{1-} \rightarrow RuO_4^{1-} + MnO_4^{2-}$	water	−0.3	−0.04	16
$TH^{\bullet+} + TTF \rightarrow TH + TTF^{\bullet+}$	acetonitrile	−0.9	−0.93	33
$DQ^{\bullet-} + BQ \rightarrow DQ + BQ^{\bullet-}$	methanol	−0.43	−0.46	34
$RuCN_6^{3-} + RuCl_6^{4-} \rightarrow RuCN_6^{4-} + RuCl_6^{3-}$	water	−1.4	−1.78[a]	tw

[a] The first two reactions involve transition-metal aqua ions. TH (thianthrene) and TTF (tetrathiafulvalene) are two organosulfur compounds which can be oxidized to stable radical cations. BQ (benzoquinone) and DQ (duroquinone) are small quinones forming radical anions. The final column gives the reference to the original papers. The last line compares the result obtained in this work (tw) to a hypothetical experimental value using the ligand additivity rules of ref 3 (see section 3.2.4).

complex and 45 (48) water molecules. The number of water molecules was chosen to guarantee vanishing mean total pressure as determined from classical simulations using parametrized interaction potentials.

Clearly the finite size and periodic boundary effects in a system of such small dimensions will be huge. Interactions with periodic images and background scale with the square of the net charge of the system. For a net charge of −4 in the reduced state these energies are in the order of 10 eV. Rather than trying to correct for such large periodic boundary effects we regard them as part of the artificial electrochemical half cell defined by our model system. Reference potential and effective ionic strength in this cell have no experimental counterpart, and half reaction energies computed from eqs 3, 4 or eq 6 have, therefore, no direct experimental significance. Reference potentials, in principle, should cancel in full redox reactions. However free energies of full reactions obtained by subtracting half reaction energies are still subject to major uncertainties related to system size effects and can also not be compared to experimental reaction free energies.

The exception is a special class of isocoulombic reactions. In this type of redox reaction the species in reactant and product have the same charges. This can be expressed schematically as

$$X^m + Y^{m+1} \rightarrow X^{m+1} + Y^m \tag{8}$$

If the species X and Y also have approximately the same spatial dimension, they will look from a distance rather similar to the solvent and image charges and the long range errors largely cancel. While there must be fundamental reasons for this compensation, the best evidence we can offer at the moment is the accuracy of the results we have obtained so far with this approach. These results are summarized in Table 1. Agreement with experimental standard potentials is good. Discrepancies are in the 100 meV range except for the ruthenate/manganate reaction, where the error is 300 meV (note that this number is still at least an order of magnitude smaller than the contributions of boundary effects to the half reaction energies).

2.4. Electronic Structure and MD Method. The electronic structure calculation methods employed here are similar to the approach used in previous ab initio MD studies of redox reactions in aqueous solutions involving transition metal ions.[15−18,31,32] The calculations were carried out using the constant-volume ab initio molecular dynamics method (Car−Parrinello scheme),[10] as implemented in the CPMD code.[36] Kohn−Sham (KS) DFT calculations were performed within the BLYP[37,38] approximation to the exchange-correlation energy. The oxidized state ($[RuCl_6]^{3-}$ and $[Ru(CN)_6]^{3-}$) was treated in the local spin density approximation constrained to doublet spin multiplicity. Norm conserving pseudopotentials (PP) according to Troullier−Martins[39] previously tested for this type of systems[15−17,40] were employed. For the construction of the Ru ion PP the electron configuration [Kr] $4d^7$ of Ru^+ is taken as a reference state, and the 4*s*, 4*p*, and 4*d* electrons are treated as valence. The pseudization radii are 1.1 au for the *s* channel, 1.2 for *p*, and 1.24 for *d*. The PPs for C, N, O, and Cl are standard atom Troullier−Martins potentials with valence *s* and *p* electrons only. The are pseudization radii $r_s = r_p = 1.23$ for C, $r_s = r_p = 1.12$ for N, $r_s = r_p = 1.05$ for O, and $r_s = 1.57$, $r_p = 1.52$ for Cl (all in a.u.). The Kleinman−Bylander scheme[41] was used for the calculation of the nonlocal part of the O, Cl, C, and N potentials, whereas the transition metal atom was treated using Gauss−Hermite integration.

Table 2: Vertical Ionization Energy ΔE (Eq 1) in eV of Vacuum $[RuCl_6]^{4-}$ and $[Ru(CN)_6]^{4-}$ Metal Complexes as a Function of the Plane Wave Cutoff (in Ry)[a]

cutoff	$[RuCl_6]^{4-}$	$[Ru(CN_6]^{4-}$
70	−9.536	−8.376
75	−9.541	−8.375
80	−9.546	−8.376
85	−9.548	−8.377
90	−9.548	−8.376
95	−9.546	−8.374

[a] The complexes have been stabilized by placing them at the center of a repulsive confining potential of cubic symmetry (eq 9). The t_{2g} (HOMO) manifold in this potential is at positive energy (see Figure 2) leading to negative ionization energy.

The KS orbitals were expanded in a plane wave (PW) basis set (Γ point only) with the kinetic energy cutoff of 70 Ry. Earlier calculations[15−17,40] on ionic solutions of ruthenium−metal complexes showed that this cutoff is sufficient for achieving a good convergence of energies and structural properties. Nevertheless, this value has been checked by computing the vertical ionization energy of the process $[ML_6]^{4-} \rightarrow [ML_6]^{3-}$ (M ≡ Ru and L ≡ Cl and CN) for the isolated (gas-phase) complex. These results are collected in Table 2 and confirm that a 70 Ry basis set is sufficiently large for the systems under study. The gas-phase calculations have been carried out in a cubic box of the same size as the MD cell used in the solution simulations (L=11.44 Å, see section 2.3). The interactions between periodic images and charge compensating homogeneous background were elimi-

Table 3: Structural Parameters of Isolated $[RuCl_6]^{4-}$ and $[Ru(CN)_6]^{4-}$ Complexes and in Aqueous Solution[a]

vacuum		solution	
$[RuCl_6]^{4-}$	$[Ru(CN)_6]^{4-}$	$[RuCl_6]^{4-}$	$[Ru(CN)_6]^{4-}$
Ru−Cl 2.63	Ru−C 2.06	Ru−Cl 2.52 (0.08)	Ru−C 2.05 (0.06)
	Ru−N 3.24	Ru−O 4.62	Ru−N 3.21 (0.06)
		Ru−H 3.71	N−H 1.8
		Cl−H 2.15	
Cl−Ru−Cl 180.	C−Ru−C 180.	Cl−Ru−Cl 174. (3.)	C−Ru−C 173. (3.)
	Ru−C−N 180.		Ru−C−N 171. (4.)

[a] Distances are in Å, angles in degrees, and uncertainties in parentheses.

nated using screening methods[42] developed for this purpose. Of course, removing all interaction with the environment is not possible in the case of multiply charged anions, since these species are unstable in a vacuum. However, because we are only interested in relative energy we have considerable freedom in the design of a convenient artificial stabilizing potential. We opted for an external potential of the form

$$V(r) = \frac{1}{2}\exp(-r) \tag{9}$$

applied at the vertices of a cube with the same size as the MD cell centered at the metal atom. This potential has the effect of confining the charge density preventing the electrons to escape. The geometry of the reduced complexes (the 4- anions) was optimized under the constraint of this potential. The resulting minimum energy structures of the $[RuL_6]^{4-}$ (L ≡ Cl or CN) metal complexes kept their octahedral symmetry with Ru−Cl, Ru−C, and Ru−N distances of 2.63, 2.06, and 3.24 Å, respectively. These and other geometry parameters are listed in Table 3. Again, these values cannot be directly compared to experimental crystal data or other theoretical estimations because they depend on our choice of external potential. We verified that the structure with CN^- bound to the ruthenium ion through the N atom is higher in energy than the C atom coordinated structure. The vertical ionization potentials of Table 2 have been evaluated for these equilibrium geometries.

The CPMD runs were carried out using a fictitious electronic mass of 500 au and a time step of 5 a.u. (0.1209 fs). Temperature was controlled by velocity scaling with a target temperature of 300 K. Every 5000 MD steps the wave function was reoptimized ("quenched") to the ground state, and the CP dynamics were restarted from the optimized wave function. This MD protocol is standard in Car−Parrinello dynamics. While adequate for the simulation of the reduced state (the solutions containing $[RuL_6]^{4-}$ L ≡ Cl, CN), we were unable to generate stable MD trajectories for the oxidized complexes using this scheme. The explanation of this instability is that the oxidized systems are open shell systems with an effectively vanishing HOMO−LUMO gap for the minority spin. The dynamical electronic optimization scheme (extended Lagrangian) used in Car−Parrinello simulation has difficulty dealing with such systems, diverging from the Born−Oppenheimer as time proceeds. This effectively prevented us from using the two-state method of eqs 6 and 7 for the estimation of the redox and reorganization free energies. These quantities have been computed instead from a trajectory of the (closed shell) reduced systems only using eqs 4 and 5.

Trajectories were around 8 ps long. Structures were saved every 10 steps for further analysis. The vertical energy gap ΔE was computed as a difference of the total energies of the $[RuL_6]^{3-}$ and $[RuL_6]^{4-}$ (L ≡ Cl, CN) complexes at the same solvent configuration generated by the ab initio MD simulation of the aqueous $[RuL_6]^{4-}$ system. At each of these configurations the total energies were computed using standard electronic optimization methods. Closed shell system energies were converged within an accuracy of 10^{-5} a.u. The convergence for the open shell system was somewhat less strict (3.5×10^{-5} a.u.).

3. Results and Discussion

3.1. Isolated Complex. The confining potential of eq 9, which was introduced in section 2.4 to test the convergence of the basis set, has the same cubic symmetry as the ligand field established by the octahedral coordination. While artificial, this system can be useful for a semiquantitative exploration of the effect of interchanging ligands in the absence of solvent. We are particularly interested in the effect on the splitting of the manifold of *d*-orbitals. The KS orbital energies in the equilibrium geometry as given in Table 3 are shown in Figure 2. Cubic symmetry labels are assigned according to the shape of the partial electron densities. From these MO diagrams, we can conclude that there is a direct correlation between the softness of the ligand and the splitting of the manifold of *d*-orbitals. We find a $e_{2g} - t_{2g}$ orbital energy gap of 0.9 eV for the Cl^- ligand and 2.3 eV for the CN^- ligand, giving a ratio of 2.6 (for further discussion see section 3.2.2).

Not only the gap between t_{2g} and e_{2g} levels in Figure 2 responds as predicted by ligand field theory but also the relative position of the HOMO levels (the t_{2g} states) reflects the difference in ligation by Cl^- and CN^-. π-acceptor bonds should be more stable than π-donor bonds, and indeed the HOMO of $[Ru(CN)_6]^{4-}$ is situated below the HOMO of $[RuCl_6]^{4-}$. Note that the value of the HOMO energy is positive ($\epsilon_{HOMO} > 0$). This is because the potential eq 9 stabilizing the intrinsically unstable anions is purely repulsive (particle in the box). This is also the explanation for the negative sign of vertical ionization potentials of Table 2. In fact the absolute values of the ionization potentials, $-IP = 9.5$ eV for $[RuCl_6]^{4-}$ and $-IP = 8.4$ eV for $[Ru(CN)_6]^{4-}$, differ only by about 1 eV from the HOMO energies of $\epsilon_{HOMO} = 10.1$ eV respectively $\epsilon_{HOMO} = 9.3$ eV in Figure 2. This

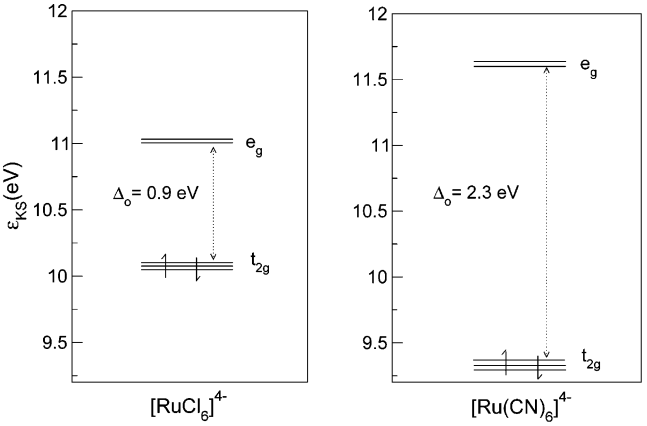

Figure 2. Kohn−Sham (KS) orbital energies of the $[RuCl_6]^{4-}$ (left) and $[Ru(CN)_6]^{4-}$ (right) complex in "vacuum". Orbital energies have been computed for optimized geometries under the influence of a confining external potential of the form $V = 1/2 \exp(-r)$ applied at the vertices of a cube centered on the metal complexes (see section 2.4). Splitting of the t_{2g} and e_{2g} manifolds is schematic and shows the number of degenerate states. Similarly the up and down half arrows indicate full occupation of the manifold.

kind of agreement between ionization potential and HOMO energy is exceptional for the BLYP functions. While in exact DFT (minus) the vertical IP and the energy of the HOMO orbital should be rigorously identical for stable closed shell molecules,[43,44] approximate density functionals such as BLYP usually give $\epsilon_{HOMO} \approx -IP/2$ (see for example ref 45, we return to the issue of the comparison of energy levels and vertical ionization energies in section 3.2.5).

3.2. Aqueous Complex. *3.2.1. Structure and Solvation.* The radial distribution functions (RDFs) for the water−metal complexes are shown in Figure 3. As a first observation, we note that the metal water RDFs (Ru−O and Ru−H) are more structured for $[RuCl_6]^{4-}$ than for $[Ru(CN)_6]^{4-}$. In fact, while the Ru−O and Ru−H RDFs for the $[RuCl_6]^{4-}$ complex show pronounced first maxima at 4.62 and 3.71 Å, it is not easy to identify any clear maximum for the $[Ru(CN)_6]^{4-}$ complex. The ligand solvent correlations as probed by the (Cl, N)−H RDFs in both the $[RuCl_6]^{4-}$ and $[Ru(CN)_6]^{4-}$ complexes show the characteristic first peaks for hydrogen bonding of water to anions. The N−H peak is somewhat stronger and at closer distance, 1.8 Å, compared to Cl−H (2.15 Å) in accordance with the difference in atomic radius. All these geometrical parameters are summarized in Table 3. Analyzing the structure in solution in more detail we see that distortions from octahedral symmetry for $[RuCl_6]^{4-}$ are only minor. The average Ru−Cl distance in the $[RuCl_6]^{4-}$ complex is 2.52 ± 0.08 Å, and the average Cl−Ru−Cl angle for Cl^- ions in the trans position is 174 ± 3°. The average Ru−C and Ru−N distances in the $[Ru(CN)_6]^{4-}$ complex are 2.05 ± 0.05 and 3.21 ± 0.06 Å, respectively, and the average C−Ru−C angle is 173 ± 3°. The important difference between the two complexes are the extra degrees of freedom due to the dimeric structure of the CN^- anion. The Ru−C−N angle undergoes substantial fluctuations in solution (see Figure 4) with an average of 171 ± 9°. The Ru, C, and N atoms are therefore (on average) not aligned, which, considering the linear Ru−C−N geometry in a vacuum, presumably means that the bending optimizes hydrogen bonding.

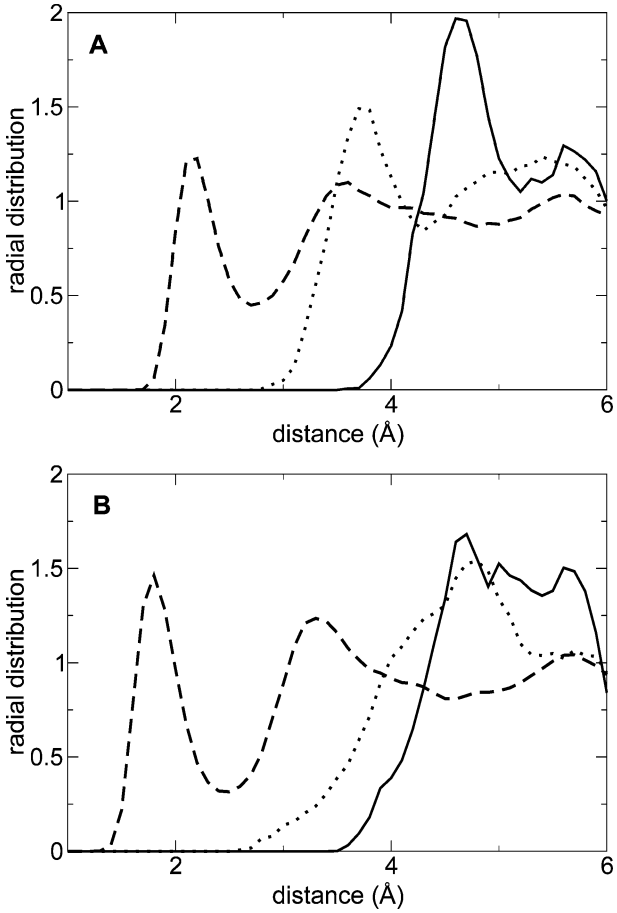

Figure 3. A: Ru−O (solid line), Ru−H (dotted line), and Cl−H (dashed line) radial distributions functions of the aqueous $[RuCl_6]^{4-}$ complex obtained from ab initio molecular dynamics simulations at 300 K. B: Ru−O (solid line), Ru−H (dotted line), and N−H (dashed line) radial distributions functions of the aqueous $[Ru(CN)_6]^{4-}$ complex obtained from ab initio molecular dynamics simulations at 300 K.

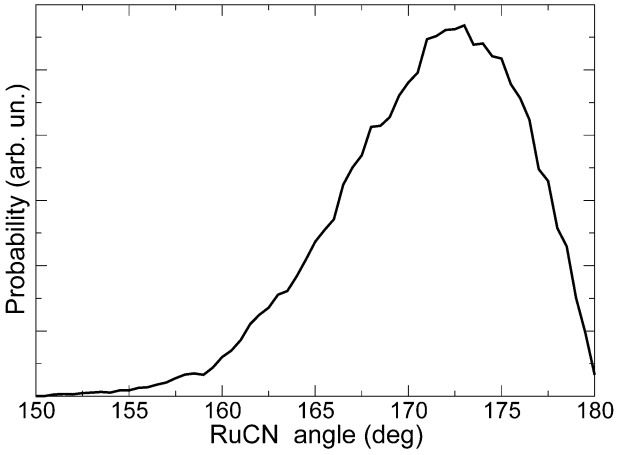

Figure 4. Distribution of the RuCN angle averaged over the aqueous $[Ru(CN)_6]^{4-}$ trajectory for which the RDF is shown in Figure 3B.

3.2.2. One-Electron Orbitals and Energies. A plot of the t_{2g} and e_g energy level scheme of the $[RuCl_6]^{4-}$ and

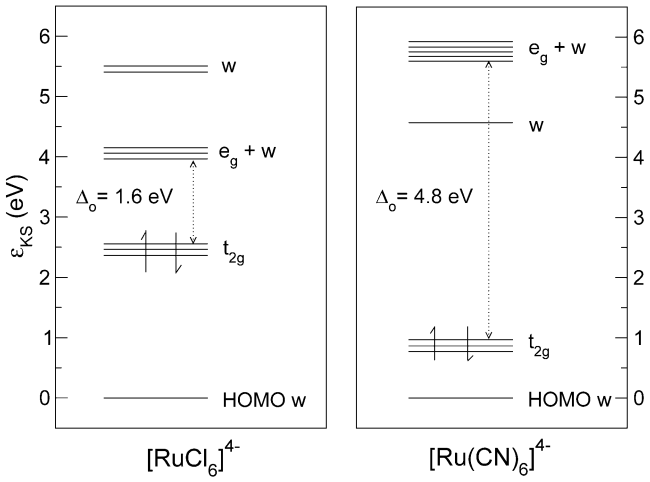

Figure 5. Kohn−Sham (KS) orbital energies of the $[RuCl_6]^{4-}$ (left) and $[Ru(CN)_6]^{4-}$ (right) complex in aqueous solution. The orbital energies have been computed for a representative configuration sampled from the ab initio molecular dynamics trajectory. The octahedral orbital symmetry labels have been assigned according to the shape of the partial electron densities (see also Figure 6). Splitting of the manifolds is schematic (see caption for Figure 2). Half arrows indicate full occupation of the HOMO. While the t_{2g} states are clearly recognizable as such (see Figure 6A), the empty e_{2g} levels are strongly mixed with solvent states (indicated by w) and have as a result very irregular contours (see Figure 6C). Δ_o is the effective octahedral crystal field splitting as obtained from the energy gap between the t_{2g} and e_{2g} manifold. The pure solvent state inserted between the t_{2g} and e_{2g} levels of $[Ru(CN])_6]^{4-}$ is depicted in Figure 6B.

$[Ru(CN)_6]^{4-}$ complexes in solution is shown in Figure 5. Also given are the energies of the highest occupied and lowest unoccupied states of the solvent. The MO diagrams are obtained by diagonalizing the KS matrix of a representative configuration sampled from the ab initio MD simulations. As KS energies in periodic systems are subject to an unphysical and system dependent shift, all one-electron energies are given relative to the HOMO of the water molecules, i.e., the top of the valence solvent band (for a rough estimate of this energy for the computational model of liquid water used here see ref 46). Using the water valence band edge as an energy reference we are assuming that its energy is not affected by the presence of a single solute. This is a rigorous property in the limit of an infinite number of solvent molecules but is an approximation in our finite size system. Comparison between different snapshots along the trajectories indicates that fluctuations in the HOMO energy are in the order of a few tenths of an eV. Symmetry labels are assigned according to the shape of the partial electron densities of the levels on the basis of the MO diagram of an octahedral ML_6 complex.

The key characteristic of the ligand field is the energy gap Δ_o induced between the e_{2g} and t_{2g} levels. The Δ_o values for the Cl^- and CN^- ligands in Figure 5 are ≈1.6 and 4.8 eV, respectively. A related piece of information contained in Figure 5 is the position of the t_{2g} and e_{2g} levels of the two species relative to the solvent states and hence, indirectly, relative to each other. We see that for both complexes the t_{2g} manifold lies well above the valence band of the solvent. Graphical rendering shows orbitals clearly recognizable as hybrid metal ligand orbitals with t_{2g}-like contours localized on the complex (Figure 6A). t_{2g} states can therefore be compared to impurity states in the gap of the solvent. This feature of the solute HOMO is shared by all aqueous transition-metal coordination complexes we have investigated so far.[16,17,22,31,47] As regards the quantative elevation of the t_{2g} levels above the water valence band, we see that for $[Ru(CN)_6]^{4-}$ the separation from the water HOMO is only ≈0.9 eV. For $[RuCl_6]^{4-}$ the solvent−solute gap is ≈2.5 eV, so substantially larger than for $[Ru(CN)_6]^{4-}$. In accordance with Figure 1 it indeed seems that in solution the t_{2g} manifolds are shifted in opposite directions, up for π-donors and down for π-acceptors (taking the valence band edge of the solvent as reference). The result is an ordering of the t_{2g} levels, $[RuCl_6]^{4-}$ (π-donor) above $[Ru(CN)_6]^{4-}$ (π-acceptor), which is also consistent with the qualitative scheme of Figure 1. Making this comparison we are of course tacitly assuming that the σ-bonding in the two complexes is similar. This assumption may be justified in view of Cl^- and CN^- ligands occupying equivalent positions in the nephelauxetic series (see for example ref 24).

Extrapolating the argument above to the empty e_{2g} manifold, one might expect on the basis of Figure 1 that these states should be rather stable and comparatively insensitive to a change of ligands. However, the e_{2g} levels, as obtained in our calculation for $[Ru(CN)_6]^{4-}$, are significantly higher in energy (>1.5 eV) compared to $[RuCl_6]^{4-}$. e_{2g} states are σ-antibonding, and it is therefore perhaps not surprising that they should be more sensitive to substitution of Cl^- by CN^- than t_{2g} states which are nonbonding for σ interactions. A complication is that the assignment is considerably more uncertain for the e_{2g} levels than it was for the t_{2g}. The reason is that mixing with virtual solvent states is much stronger, in particular with the solvent LUMO. In pure water model systems of the size used here this state appears as a discrete energy level ≈4.5 eV above the water HOMO ($1b_1$) band.[22,47,48] This state is effectively degenerate with the $RuCl_6^{4-}$ e_{2g} states. Interactions are strong, and it is in practice not possible to distinguish between the three levels in the manifold assigned as e_{2g} + w in Figure 5.

The water LUMO is also the dominant component in the (single) state observed in the orbital diagram of $[Ru(CN)_6]^{4-}$ at approximately the same energy (4.5 eV) as for $[RuCl_6]^{4-}$. However, while there is some hybrization with CN^- orbitals, this state has negligible metal *d* character (Figure 6B). Metal *d* character only appears at higher energies (>5.5 eV). This prompted us to locate the e_{2g} levels there, although none of these states has a clear resemblance to textbook e_{2g} orbitals and all of them are mixed with empty delocalized ("conduction") states of the solvent (Figure 6C). There is general agreement that the gap in the density of states of liquid water is underestimated by at least 2 eV by the BLYP functional.[22,47,48] Most of the phenomenology of the e_{2g} levels described above must therefore be considered an artifact of the DFT approximation employed in this calculation.[49] This

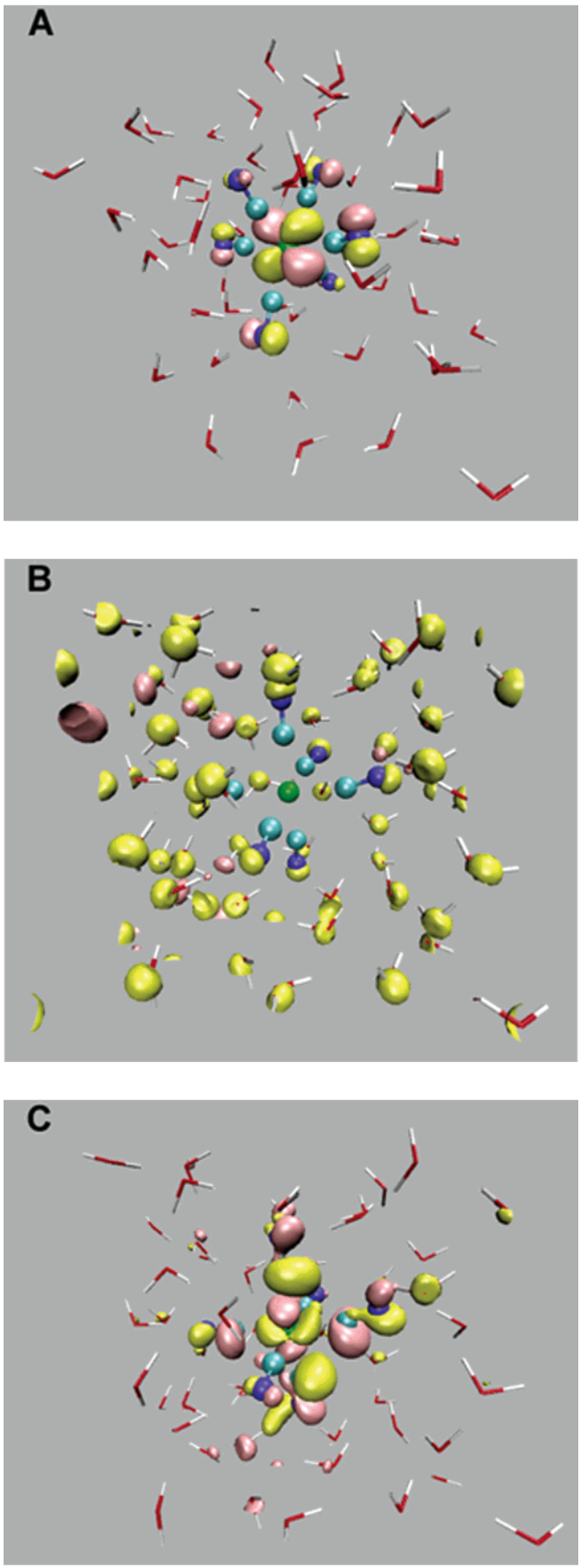

Figure 6. Isosurfaces of molecular orbitals of aqueous $[Ru(CN)]_6]^{4-}$. A: t_{2g} state (HOMO), localized on complex. B: LUMO, mainly solvent. C: e_{2g}-like (LUMO+1), complex + solvent. For the corresponding orbital energies see Figure 5.

Table 4: Literature Values for Crystal Field Splitting Parameter Δ_o in eV for Several Octahedral $M^{2/3+}$ L_6, L = Cl^-, CN^- Transition Metal Compounds[a]

	conf	Cl^-	CN^-
Fe^{2+}	$3d^6$		4.1
Co^{3+}	$3d^6$		4.2
Rh^{3+}	$4d^6$	2.5	
Ir^{3+}	$5d^6$	3.1	
Ru^{2+}(tw)	$4d^6$	1.6	4.8

[a] Data were taken from ref 24. The last line gives the estimates calculated for Ru^{2+} in this work (tw) from the gap in the KS one-electron levels in aqueous solution.

also represents a major source of uncertainty in our estimation of the crystal field parameter Δ_o.

Direct validation of the computed values of Δ_o by experiment is difficult because of the lack of data for Ru complexes. However, the CN^-/Cl^- ratio of 3 for the Δ_o in Figure 5 substantially exceeds the estimate of 2.2 compiled by Jorgensen using spectrochemical data of a series of coordination complexes.[23] Trends for hexachlorides and cyanides of related group VIII and IX transition metals can give a more detailed indication of the accuracy of our results. In Table 4 we have collected some relevant examples. The cyanide data suggest that our value of 4.8 eV for the $[Ru(CN)_6]^{4-}$ could in fact be realistic. Because Δ_o increases when going down from first to second row, the experimental numbers in the table must therefore be considered as a lower bound for the Ru complex. Our value of 1.6 eV for $[RuCl_6]^{4-}$ is more suspect and is most likely a significant underestimation, which would be consistent with the overestimation of the Δ_o CN^-/Cl^- ratio.

The discussion above is based on a direct comparison of KS orbital energy difference $\Delta\epsilon = \epsilon_{eg} - \epsilon_{t2g}$ to experimental crystal field parameters Δ_o obtained from electronic absorption spectroscopy. However, it is well-known that transitions between t_{2g}^6 and $t_{2g}^5e_g$ configurations give rise to two spectroscopic terms at different energies corresponding to excitation from the $^1A_1$ ground state to a $^1T_1$ and $^1T_2$ state. This introduces a further uncertainty in our estimation of Δ_o. This question was investigated in some detail in a time dependent density functional theory (TDDFT) study of the optical spectrum of the $Ru^{2+}(H_2O)_6$ complex in aqueous solution.[22] Analyzing the TDDFT absorption spectrum using the Sugano-Tanabe method (see e.g. ref 24) we obtained a octahedral crystal parameter of $\Delta_o = 2.23$ eV. This value is close to the KS energy gap of $\Delta\epsilon = 2.1$ eV we found for this system confirming that the KS energy gap is a reliable measure for crystal field parameter. Subjecting the experimental absorption spectrum to the same analysis gives $\Delta_o = 2.73$ eV. Since the DFT technology (BLYP functional, plane-wave basis set, and pseudopotentials) used in the Ru aqua-ion study is identical to the approach applied here, the discrepancy of $\approx$0.5 eV can be considered as a fair estimate of the error in our calculation of Δ_o. We also note that the BLYP value for Δ_o of the hexahydrate is too low, which is consistent with the current results for $[RuCl_6]^{4-}$ (see above).

3.2.3. Spin and Electron Densities. The density of unpaired electrons is observable as spin density by means of EPR techniques.[50,51] Spin density in DFT is defined as ρ_β-ρ_α, ρ_β,

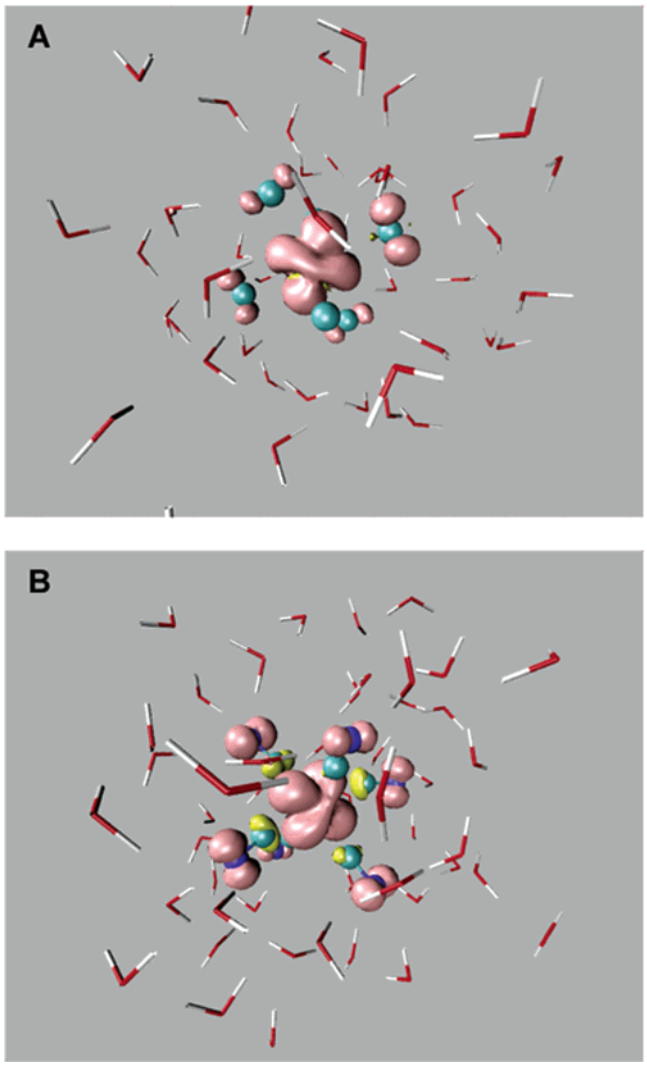

Figure 7. Isosurfaces corresponding to the spin density defined as ρ_β-ρ_α, with ρ_β and ρ_α being the electronic density of the β (minority spin) and α (majority spin) electrons of the aqueous $[RuCl_6]^{3-}$ complex (A) and $[Ru(CN)_6]^{3-}$ complex (B). The yellow isosurface indicates an excess of ρ_β of 0.002 a.u.$^{-3}$, and the pink isosurface indicates an excess of ρ_α of 0.002 a.u.$^{-3}$.

and ρ_α being the electronic density of the β and α electrons as obtained from an unrestricted KS calculation. The Ru(III) coordination complexes are doublets in a t_{2g}^5 configuration. The spin density therefore probes the spatial extent of a hole in the t_{2g} manifold. It contains information about the π-bonding of metal and ligand orbitals and may therefore be able to differentiate between the two complexes. In Figure 7 we show the spin density of the $[RuCl_6]^{3-}$ and $[Ru(CN)_6]^{-3}$ metal complexes in solution after vertical ionization. It can be seen that the spin density is delocalized over metal and ligand atoms but is not spilling out to the solvent molecules consistent with the orbital picture discussed in section 3.2.2. The most pronounced accumulation of spin density is concentrated on the ruthenium atom with contours of t_{2g} shape (compare Figure 6A). The smaller fraction of the spin density residing on the ligands also clearly reflects the π orbital character of the hole. Note that in the case of $[Ru(CN)_6]^{3-}$ the spin density on the C atoms has a sign

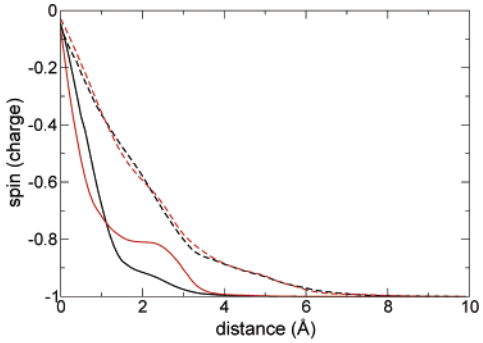

Figure 8. Radial extension of the electron hole in the aqueous $[RuCl_6]^{3-}$ (black) and $[Ru(CN)_6]^{3-}$ (red) complexes. Given are the radial integrals of the average spin density according to eq 10 (solid lines) and vertical charge difference densities (dashed lines) as a function of the distance to the ruthenium ion. For snapshots of the corresponding densities see Figures 7 and 9.

opposite to the majority spin. Technically, this effect arises as a consequence of spin polarization in the unrestricted KS scheme and may or may not be a DFT artifact (for a discussion of these issues see for example refs 50 and 51).

For a more quantitative characterization we have investigated the average spin density $\zeta(r)$ as a function of the distance r to the ruthenium metal. Rather than the radial distribution $\zeta(r)$ we plot in Figure 8 the radial integral $n_\sigma(r)$ formally defined as

$$n_\sigma(r) = 4\pi \int_0^r \mathrm{d}r'(r')^2\zeta(r') \qquad (10)$$

For doublet states we should have in our convention $n_\sigma(r \rightarrow \infty) = -1$. From Figure 8 we can conclude that the spin density is more spread out in $[Ru(CN)_6]^{3-}$ than in $[RuCl_6]^{3-}$. This observation can be interpreted as evidence of a "bigger hole" in the case of the $[Ru(CN)_6]^{3-}$ complex due to the π-acceptor character of the CN^- ligands, which allows for net electron transfer to the ligands. Comparison to the RDFs in Figure 3 confirms that the spin density is largely confined to the complex. For both complexes the integrated spin density has reached -1 at the minimum Ru−O distance $r_{cO} \approx 3.5$ Å as estimated from the corresponding RDF in Figure 3. However, there is a small overlap between the radial spin density and Ru−H RDF. If spin density beyond a coordination radius $r_{cH} = 3.0$ Å can be regarded as effectively transferred to the solvent, the results for $[Ru(CN)_6]^{3-}$ would indicate that about 10% of the hole resides on the water H atoms. This interpretation, however, is far from certain, and a more detailed analysis of the hydrogen bonding to the nitrogen atoms is necessary.

A further quantity of interest is the vertical electronic density hole, defined as the electron density of the oxidized state (ρ_O) minus the electronic density of the reduced state (ρ_R) at the same atomic configuration (solute + solvent). While spin density and electronic density holes are not independent quantities, it has been frequently observed that they highlight rather different aspects of the bonding. This is nicely illustrated by Figure 9 which shows the electron density hole for the same configuration as used in Figure 7 for the visualization of the spin density. In the case of

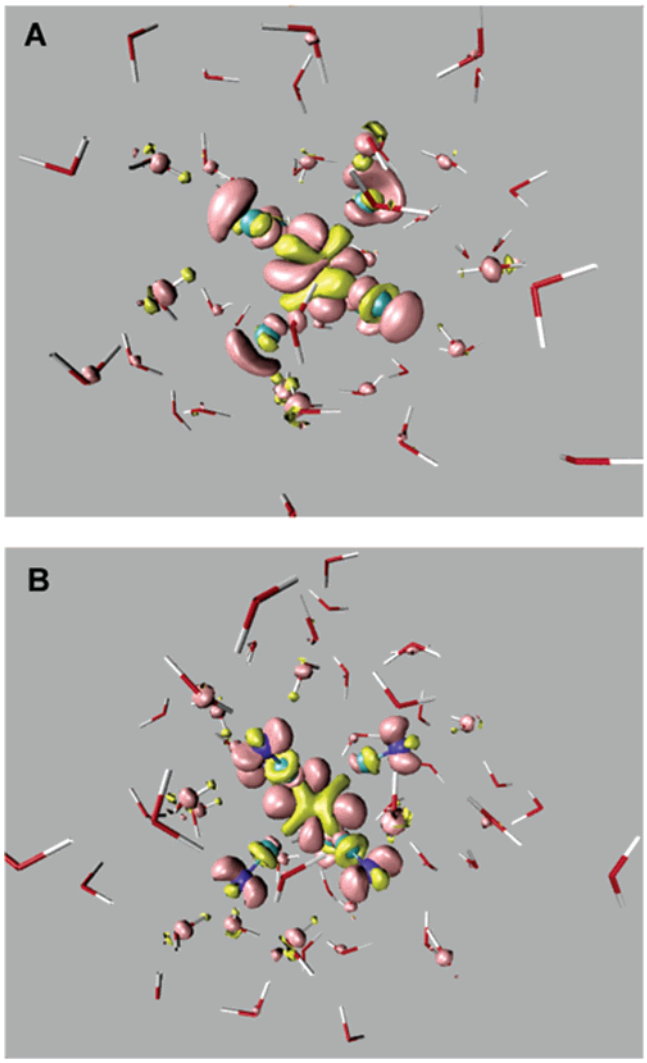

Figure 9. Isosurfaces corresponding to the vertical charge difference density defined as $\rho_O - \rho_R$, with ρ_O and ρ_R being the electronic density of the oxidized and reduced states at the same solvent configuration. Part A shows the result of an instantaneous configuration of the aqueous $[RuCl_6]^{3-}$ complex and part B for the $[Ru(CN)_6]^{3-}$ complex. The yellow isosurface indicates an excess of ρ_O of 0.002 a.u.$^{-3}$, and the pink isosurface indicates an excess of ρ_R of 0.002 a.u.$^{-3}$. Note the change in polarization of the solvent.

$[Ru(CN)_6]^{4-}$ the main features reflect the spin density (Figure 7) except for the contribution of the solvent which is due to changes in the polarization (see below). It can be seen that most of the charge removed by (vertical) ionization comes from π bonds. The picture for $[RuCl_6]^{4-}$, in contrast, shows very little π character. If anything, the electron density hole for the chloride resembles the charge density of σ bonds. These results support an electronic structure model in which the bonding in Cl^- and CN^- compounds has a rather different origin.

For a quantitative analysis we introduce a radially integrated electron hole density $n_\rho(r)$ similar to the radial spin integral of eq 10. Again $n_\rho(r \rightarrow \infty) = -1$, hence $n_\rho(r)$ and $n_\sigma(r)$ can be directly compared (Figure 8). Unlike the spin densities, we find that the electronic difference densities are virtually identical for the two complexes. The radial dependence also shows little structure distinguishing between metal and ligand. The discontinuity in the derivative ("bend") at $r \approx 3.5$ Å coincides with the radius of minimum approach r_{cO} between the metal center and the solvent oxygen atoms in the RDFs of Figure 3. This confirms that $r = 3.5$ Å marks the transition between solute and solvent. Using this distance as a measure of the size of the complex, Figure 8 seems to suggest that around 85% of the electron density hole is on the solute (for both complexes). However, going back to Figure 9 we see that a good fraction of the charge density hole in the solvent can be explained by the electronic dielectric response of the solvent to the oxidation of the solute. Because of polarization by the negatively charged solute, solvent molecules that are not fully included inside the integration sphere will contribute a net charge to the spherical integral with a sign opposite to the charge of the ionic solute at the center of the sphere. The result is a sphere with a (reduced) screened charge, which will of course adjust to a change of charge of the solute when oxidized, contributing in this way to the charge density hole. This argument also underlines our observation about differences in the information contained in spin and charge density holes.

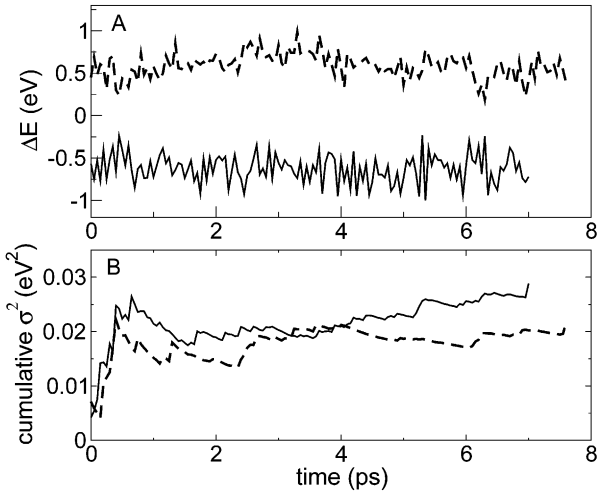

Figure 10. Vertical ionization energy ΔE (eq 1) obtained from ab initio molecular dynamics simulations of the aqueous $[RuCl_6]^{4-}$ complex (solid line) and $[Ru(CN)_6]^{4-}$ complex (dashed line). Part A shows the time series of ΔE and part B the cumulative variance.

3.2.4. Thermodynamic Properties. The time evolution of the vertical oxidation energy ΔE is displayed in Figure 10. This quantity was computed according to eq 1 as the difference of the total energies of the $[RuL_6]^{3-}$ and $[RuL_6]^{4-}$ (L ≡ Cl, CN) complexes. For given solute + solvent configuration the wave function of the oxidized and reduced states were quenched to the Born−Oppenheimer surface (eliminating possible inaccuracies related to Car−Parrinello dynamics). The configurations were sampled from a trajectory of the reduced complex ($[RuL_6]^{4-}$). Averages ΔE_R show a clear dependence on the ligands. We find $\Delta E_R = -0.62$ eV for Cl^- and $\Delta E_R = 0.59$ eV for CN^-. The fluctuations of the vertical energy gap are more similar, giving $\sigma_R^2 = 0.03$ eV^2 for Cl^- and $\sigma_R^2 = 0.02$ eV^2 for CN^-. Converting variances to reorganization free energies using eq 5 we obtain $\lambda = 0.6$ eV for the $[RuCl_6]^{3/4-}$ reaction and $\lambda = 0.4$ eV for the $[Ru(CN)_6]^{3/4-}$ reaction. These results are summarized in

Table 5: Summary of the Results Obtained for the Energetics and Thermochemistry by Averaging over Trajectories of the Reduced Systems[a]

	ΔE_R	λ	ΔA
$[Ru(CN)_6]^{3/4-}$	0.59	0.4	0.2
$[RuCl_6]^{3/4-}$	−0.62	0.6	−1.2

[a] ΔE_R is the vertical ionization energy (eq 1), λ is the reorganization energies computed from the gap fluctuations according to eq 5, and ΔA is the resulting estimate of the free energy of oxidation using eq 4.

Table 5 for later reference. Inserting the estimates for ΔE_R and λ in eq 4 leads to a $\Delta A = -1.2$ eV for oxidation of the $[RuCl_6]^{4-}$ complex and $\Delta A = 0.2$ eV for the $[Ru(CN)_6]^{4-}$ complex. Recalling that free energies of oxidation (eq 2) have the same sign as reduction potentials, we conclude that according to our results $[Ru(CN)_6]^{3-}$ is a much stronger oxidant than $[RuCl_6]^{3-}$. Indeed the difference in half reaction energies predicts a strongly exergonic reaction free energy change of $\Delta\Delta A = -1.4$ eV for the full $[RuCl_6]^{4-} + [Ru(CN)_6]^{3-} \rightarrow [RuCl_6]^{3-} + [Ru(CN)_6]^{4-}$ redox reaction.

Before attempting a comparison to experiment we first comment on the statistical uncertainties in our estimate for the oxidation free energy. As discussed in section 2.2 the drawback of the use of eq 4 is the slow convergence of the time average of the variance and hence the reorganization free energy (eq 5). Indeed, as can be seen from Figure 10B the statistical uncertainty in the estimate for the variance is in the order of 25%. For an independent assessment of this error we have performed a 1 ps run of the $[RuCl_6]^{3-}$ system at a reduced time step and suppressing the instability of the molecular dynamics of this open shell system by Nosé thermostats applied to both the ionic and fictitious electronic degrees of freedom (unfortunately this approach was considerably less effective for the stabilization of the open-shell Ru cyanide complex). The value of the vertical gap by averaging over this short trajectory of the chloride complex is $\Delta E_O = -1.3$ eV. Substituting this together with the ΔE_R of the 8 ps run (Table 5) in eq 6 we find an oxidation free energy $\Delta A = -1.0$ eV. The discrepancy with value of $\Delta A = -1.2$ eV computed using eq 4 suggests that the error in our estimate of redox free energy is approximately 0.2−0.3 eV.

The standard reduction potential of the aqueous $[Ru(CN)_6]^{4/3-}$ couple (as measured against the standard hydrogen electrode) is 0.9 V.[52] The oxidative nature of the cyanide complex as found in our calculation is therefore supported by experiment. However, as mentioned in section 2.3 the half reaction free energies computed by our method cannot be directly compared to experimental reduction potentials. Only free energies changes of full reactions are meaningful and then only for isocoulombic reactions (see eq 8). The $[Ru(CN)_6]^{3/4-}$ and $[RuCl_6]^{3/4-}$ reactions satisfy this condition, but, unfortunately, the $[RuCl_6]^{4/3-}$ metal complexes are not stable in aqueous solution against ligand-solvent exchange. Nonaqueous solvents, however, stabilize a large variety of cyanide and chloride complexes mixed with a host of other ligands.[2,3] Lever has used this vast database to parametrize a simple linear ligand additivity model capable of describing the experimental redox potentials with remarkable accuracy.[3,4] The model can be formulated by the following expression for the observed reduction Ru(III)/Ru(II) potential E_{obs} in units of V

$$E_{obs} = \sum_i E_L(L_i) + C \tag{11}$$

where the summation is over the various ligands L_i of the complex. C is a constant depending on the reference electrode. The E_L parameters given in ref 3 for CN^- and Cl^- are $E_L(CN^-) = 0.12$ V and $E_L(Cl^-) = -0.24$ V. This would yield according to eq 11 a free energy for the full $[RuCl_6]^{4-} + [Ru(CN)_6]^{3-} \rightarrow [RuCl_6]^{3-} + [Ru(CN)_6]^{4-}$ redox reaction of $\Delta\Delta A_{obs} = -1.56$ eV. While our computed value of $\Delta\Delta A = -1.4$ eV is very close, the two redox potentials are not equivalent because the E_L coefficients are strictly valid only for reactions in acetonitrile solution. Reference 3 also gives an empirical rule for the conversion to aqueous solution, amounting to multiplication by a factor of 1.14. Applying this correction the predicted value increases to $\Delta\Delta A_{obs} = -1.78$ eV. Using this value as our experimental reference we conclude that the calculation underestimates the absolute reaction free energy change by ≈0.4 eV.

3.2.5. Redox Potentials and One-Electron Energy Levels. We are now ready to return to the issue raised in the Introduction, namely the question of a possible correlation between one-electron energies and the redox potential. As mentioned in section 3.2.2 such a correlation exists for stable finite systems in a vacuum. The HOMO energy (ϵ_{HOMO}) as computed for the (unknown) exact density functional is rigorously equal to the (minus) vertical ionization energy (IP).[43,44] However, for the approximate density functionals of the type used here (generalized gradient corrections) this relation is far from satisfied: $-\epsilon_{HOMO}$ is found to be considerably smaller than IP, usually only half this value.[45] The first question is, therefore, how the energy of the redox active orbitals of the reduced extended system compares to the vertical energy gap. Taking, as explained in section 3.2.2, the top edge of the solvent valence band as reference and subtracting the t_{2g} energy of $[RuCl_6]^{4-}$ from the corresponding energy for $[Ru(CN)_6]^{4-}$ we obtain a value of $\Delta\epsilon_{t2g} = -1.6$ eV. This number should be compared to the difference in vertical energy gap (Table 5) $\Delta\Delta E_R = 1.2$ eV. We find that in our solution model system $-\Delta\epsilon_{HOMO}$ differs from $\Delta\Delta E_R$ by about 30%. While this discrepancy is appreciable, it is significantly smaller than the mismatch observed for BLYP for ionization under vacuum conditions. We note that our calculations reported in ref 16 of the $MnO_4^{2-} + RuO_4^{1-} \rightarrow MnO_4^{1-} + RuO_4^{2-}$ aqueous redox reaction gave a very similar result, namely $-\Delta\epsilon_{HOMO} = 0.7$ eV versus $\Delta\Delta E_R = 0.4$ eV.

Comparing next the KS HOMO energy gap $\Delta\epsilon_{HOMO} = -1.6$ eV to the free energy change $\Delta\Delta A = -1.4$ eV computed for the full (reverse) redox reaction, we find an even better agreement. KS energy gaps and reaction free energies have a rather different thermodynamic status, and to understand the relation between these two quantities we go back to the discussion in section 3.2.4 and recall our observation that ligand character has a far more pronounced effect on the vertical ionization than on the relaxation of the

system after the ET process. We found the reorganization free energies to be rather similar ($\Delta\lambda = -0.2$ eV, see Table 5). To see what this implies for the thermochemistry we substitute eq 4 in the expression for the reaction free energy of the full reaction and obtain

$$\Delta\Delta A = \Delta\Delta E_R - \Delta\lambda \tag{12}$$

Setting $\Delta\lambda \approx 0$ gives $\Delta\Delta A \approx \Delta\Delta E_R$. On the condition that the KS HOMO energy gap is a good approximation to the vertical ionization difference, the correspondence with the redox free energy is therefore a consequence of cancellation of the reorganization energies.

4. Concluding Remarks

The density functional MD simulations reported in this paper confirm that the higher oxidation state of the metal ion, Ru(III), is more stable when chelated by Cl^- than by CN^- ligands. This is in agreement with the conventional ligand field picture sketched in section 2.1. Due to the differences in π-bonding, oxidation of $[Ru(CN)_6]^{4-}$ amounts to removing an electron from a bonding t_{2g} HOMO. In the $[RuCl_6]^{4-}$ complex this orbital has changed character to π-antibonding, and we can expect that removing an electron from this orbital should be energetically less costly. We also found, that within a margin of a few tenths of eV, the gap between the HOMO energy levels of reactants could be used as an estimate of the free energy change of the full redox reaction. This near quantitative correlation between the orbital level scheme and thermochemistry was traced to a combination of cancellation of reorganization effects and the relatively close agreement between vertical ionization energy differences and KS energy gaps. Of these two observations, the latter is perhaps the more surprising. We note, however, that this agreement, while exceptional for vacuum systems, is not uncommon in extended metallic systems, where the work function can often be estimated to a very good approximation by the Fermi energy as computed for a slab of material using common approximate density functionals.[53] This suggests that the degree of localization of the redox active orbital may play an important role. This explanation, however, must remain at the moment rather speculative, and it would be useful to investigate whether similar conditions apply to other related coordination compounds and, if so, why. To conclude we comment on the accuracy of our result for redox free energy. Clearly an absolute error of 0.4 eV is larger than one would like (note, however, that this is the most unfavorable case in Table 1). There are three main sources for this error: insufficient convergence of statistics, size effects, and the level of approximation of the density functional calculations. Run length was of particular concern in the present calculation as it required the estimation of the second moment of fluctuations for the computation of reaction and reorganization free energy (eqs 5 and 4). This statistical uncertainty can be reduced substantially by the use of the two surface expressions (eqs 6 and 7). This was not feasible in the present Car−Parrinello simulation because of the near degenerate open shell character of one of the oxidation states. These difficulties can however be eliminated by switching to Born−Oppenheimer dynamics.[33] While size effects on half reaction energies are huge, they cancel to a large extent for the full reaction studied here. The chemistry controlling redox reactions is essentially short range. Figure 8 gave a nice illustration supporting this claim. The difference charge density determining the long range electrostatic component of the reaction energy is virtually the same for the chloride and cyanide complex. We are therefore fairly confident that size effects are not the main cause of the error. Further investigations are however needed.

The performance of the DFT is more difficult to assess. If the correlation between redox potentials and HOMO energy levels can be taken seriously, which seems a possibility at least for our system, then we can use the one-electron density of states to analyze the redox chemistry. Such an analysis suggests that the $[RuCl_6]^{4-}$ HOMO levels (the t_{2g} manifold in Figure 5) are too low in energy. Moving these levels up while leaving the t_{2g} levels of $[Ru(CN)_6]^{4-}$ where we found them (Figure 5) would increase the redox free energy bringing the DFT estimation in better agreement with experiment. Assuming that also the empty e_{2g} stay fixed, a higher t_{2g} energy would also reduce the crystal field splitting for the hexachloride complex, which came out too high in our calculation (section 3.2.2). We see, however, for the moment no convincing reason why the HOMO energy of the aqueous ruthenium chloride complex should be less reliable than for the cyanide complex. Increased interaction with the empty solvent states which we know are too close in energy to the occupied states could be a possibility. We are however optimistic that the more technical aspects of the simulation, sampling and system size, can be improved and related errors reduced making a detailed analysis of the relation between thermochemistry and electronic structure both meaningful and helpful for the understanding of the performance of DFT in condensed molecular systems.

Acknowledgment. This research is sponsored by EPSRC and HPC-Europe. R.A. is grateful to the Spanish government (MEC) and Marie Curie Fellowship for financial support. R.A. thanks the molecular modeling group at ICMAB, specially Lourdes F. Vega, for the warm hospitality during her stay at Barcelona. Part of the computations was carried out on BSC facilities.

References

(1) Bargeletti, F.; Juris, A.; Balzani, V.; Belser, P.; von Zelewsky, A. *Inorg. Chem.* **1987**, *26*, 4115−4119.

(2) Juris, A.; Balzani, V.; Barigelleti, F.; Campagna, S.; Belser, P.; von Zelewsky, A. *Coord. Chem. Rev.* **1988**, *84*, 85−277.

(3) Lever, A. B. P. *Inorg. Chem.* **1990**, *29*, 1271−1285.

(4) Lever, A. B. P.; Dodsworth, E. S. In *Inorganic Electronic Structure and Spectroscopy*; Solomon, E. I., Lever, A. B. P., Eds.; John Wiley and Sons: New Jersey, 1999; Vol. II, Chapter 4, p 227.

(5) Siegbahn, P. E. M. *Adv. Chem. Phys.* **1996**, *93*, 333−387.

(6) Li, J.; Fisher, C. L.; Chen, J. L.; Bahford, D.; Noodleman, L. *Inorg. Chem.* **1996**, *35*, 4694−4702.

(7) Martinez, J. M.; Pappalardo, R. R.; Sánchez Marcos, E.; Mennucci, B.; Tomasi, J. *J. Phys. Chem. B* **2002**, *106*, 1118−1123.

(8) Angelis, F. D.; Tilocca, A.; Selloni, A. *J. Am. Chem. Soc.* **2004**, *126*, 15024−15025.
(9) Rustad, J. R.; Dixon, D. A.; Rosso, K. M.; Felmy, A. R. *J. Am. Chem. Soc.* **1999**, *121*, 3234−3235.
(10) Car, R.; Parrinello, M. *Phys. Rev. Lett.* **1985**, *55*, 2471−2474.
(11) Ikeda, I.; Hirata, M.; Kimura, T. *J. Chem. Phys.* **2003**, *119*, 12386−12392.
(12) Ikeda, I.; Hirata, M.; Kimura, T. *J. Chem. Phys.* **2005**, *122*, 024510.
(13) Amira, S.; Spångberg, D.; Zelin, V.; Probst, M.; Hermansson, K. *J. Phys. Chem. B* **2005**, *109*, 14235−14242.
(14) Ensing, B.; Buda, F.; Blochl, P. E.; Baerends, E. J. *Phys. Chem. Chem. Phys.* **2002**, *4*, 3619−3627.
(15) Blumberger, J.; Sprik, M. *J. Phys. Chem. B* **2005**, *109*, 6793−6804.
(16) Tateyama, Y.; Blumberger, J.; Sprik, M.; Tavernelli, I. *J. Chem. Phys.* **2005**, *122*, 234505.
(17) Blumberger, J.; Sprik, M. *Theor. Chem. Acc.* **2006**, *115*, 113−126.
(18) Blumberger, J.; Tavernelli, I.; Klein, M. L.; Sprik, M. *J. Chem. Phys.* **2006**, *124*, 064507.
(19) Warshel, A. *J. Phys. Chem.* **1982**, *86*, 2218−2224.
(20) Hwang, J.-K.; Warshel, A. *J. Am. Chem. Soc.* **1987**, *109*, 715−720.
(21) King, G.; Warshel, A. *J. Chem. Phys.* **1990**, *93*, 8682−8692.
(22) Bernasconi, L.; Sprik, M. *J. Phys. Chem. B* **2005**, *109*, 12222−12226.
(23) Jorgensen, C. K. *Modern aspects of ligand field theory;* North-Holland: Amsterdam, 1971.
(24) Bersuker, I. B. *Electronic structure and properties of transition metal compounds*; Wiley & Sons: 1996.
(25) Marcus, R. A. *J. Chem. Phys.* **1956**, *24*, 966−978.
(26) Marcus, R. A. *J. Chem. Phys.* **1956**, *24*, 979989.
(27) Marcus, R. A. *J. Chem. Phys.* **1957**, *26*, 867−872.
(28) Marcus, R. A. *J. Chem. Phys.* **1965**, *43*, 679−701.
(29) Marcus, R. A.; Sutin, N. *Biochim. Biophys. Acta* **1985**, *811*, 265322.
(30) Marcus, R. A. *Rev. Mod. Phys* **1993**, *65*, 599−610.
(31) Blumberger, J.; Bernasconi, L.; Tavernelli, I.; Vuilleumier, R.; Sprik, M. *J. Am. Chem. Soc.* **2004**, *126*, 3928−3938.
(32) Blumberger, J.; Sprik, M. *J. Phys. Chem. B* **2004**, *108*, 6529−6535.
(33) VandeVondele, J.; Lynden-Bell, R.; Meijer, E. J.; Sprik, M. *J. Phys. Chem. B* **2006**, *110*, 3614−3623.
(34) VandeVondele, J.; Sulpizi, M.; Sprik, M. *Angew. Chem., Int. Ed.* **2006**, *45*, 1936−1938.
(35) Tachiya, M. *J. Phys. Chem.* **1989**, *93*, 7050−7052.
(36) CPMD Version 3.9.2, Copyright IBM Corp 1990−2001, Copyright MPI fur Festkorperforschung Stuttgart 1997−2005.
(37) Becke, A. *Phys. Rev. A* **1988**, *38*, 3098−3100.
(38) Lee, C.; Yang, W.; Parr, R. *Phys. Rev. B* **1988**, *37*, 785−789.
(39) Troullier, N.; Martins, J. *Phys. Rev. B* **1991**, *43*, 1993−2006.
(40) Blumberger, J.; Tateyama, Y.; Sprik, M. *Com. Phys. Comm.* **2005**, *169*, 256−261.
(41) Kleinman, L.; Bylander, D. *Phys. Rev. Lett.* **1982**, *48*, 1425−1428.
(42) Martyna, G.; Tuckerman, M. *J. Chem. Phys.* **1999**, *110*, 2810−2821.
(43) Almbladh, C. O.; von Barth, U. *Phys. Rev. B* **1985**, *31*, 3231−3244.
(44) Chong, D. P.; Gritsenko, O. V.; Baerends, E. J. *J. Chem. Phys.* **2002**, *116*, 1760−1772.
(45) Grüning, M.; Gritsenko, O. V.; van Gisbergen, S. J.; Baerends, E. J. *J. Chem. Phys.* **2002**, *116*, 9591−9601.
(46) Hunt, P.; Sprik, M. *Chem. Phys. Chem.* **2005**, *6*, 1805−1808.
(47) Bernasconi, L.; Blumberger, J.; Sprik, M.; Vuilleumier, R. *J. Chem. Phys.* **2004**, *121*, 11885−11899.
(48) Pendergast, D.; Grossman, J. C.; Galli, G. *J. Chem. Phys.* **2005**, *123*, 014501.
(49) An added complication is that the Γ point-only *k* space sampling as applied here is likely to be not adequate for the delocalized virtual solvent states.[48] Introduction of more *k* points may therefore affect the energies of these states and, hence, the mixing with the localized virtual states of the solute.
(50) Improta, R.; Barone, V. *Chem. Rev.* **2004**, *104*, 1231−1245.
(51) Remenyi, C.; Kaupp, M. *J. Am. Chem. Soc.* **2005**, *127*, 11399−11413.
(52) Bard, A.; Parsons, R.; Jordan, J. *Standard Potentials in Aqueous Solutions;* IUPAC: New York, 1985.
(53) Lozovoi, A. Y.; Alavi, A. *Phys. Rev. B* **2003**, *68*, 245416.

CT600169E